*J. Min. Metall. Sect. B-Metall., 56 (3) (2020) 337 - 351*

**Journal of Mining and Metallurgy, Section B: Metallurgy**

# INFLUENCE OF IRON ORE CONCENTRATE ON THE CHARACTERISTICS OF SINTERING AND REDUCTION OF SINTER

**H. Guo [a], F.-M. Shen [b], X. Jiang [b,*], D.-W. Xiang [b], H.-Y. Zheng [b]**

[a] Hebei North University, Zhangjiakou, Hebei, China
[b] School of Metallurgy, Northeastern University, Shenyang, Liaoning, China

*(Received 21 February 2019; accepted 29 September 2020)*

***Abstract***

*As Australia is the main iron ore importing country for China, the abundant mineral resources of Australia are the primary raw materials for the sintering process. To better understand the properties of different iron ores from Australia and then guide the sintering process, this study selected four types of Australian ore and one type of domestic ore, and their properties were investigated under different conditions. The experiment of single iron ore sintering was studied to examine the influence of different iron ores on the metallurgical properties of sinter. From this study, the following results were obtained: GG showed poor fluidity and higher assimilability temperature, but the bonding phase strength was the highest; YD showed better fluidity and lower assimilability temperature, whereas SJY (domestic ore) showed better fluidity and higher bonding phase strength, and lower assimilability temperature. The influence mechanism of iron ore on the fluidity was further analyzed by using SEM and ion theory of slag. With the increase $SiO_2$ content of iron ore, the fluidity index increased, the main reason was that the amount of liquid phase increased and the melting point decreased during the sintering. However, an excessive amount of $SiO_2$ caused the decrease of fluidity index of iron ore; the main reason was that the fluidity of the liquid phase itself decreased and secondary hematite appeared. In the case of the higher $SiO_2$ content of iron ore, the main bonding phase was calcium silicate. With the decrease of $SiO_2$ content, the calcium silicate transformed into calcium ferrite. The main reason for this was that the Gibbs free energy of calcium ferrite and dicalcium ferrite ($2CaO{\cdot}SiO_2$) was higher than that of calcium silicate in the temperature ranges of 400-1600 K. The reduction degree of YD was the highest in all the cases and that of GG was the lowest. Activation energies of 5.39, 3.14, 3.51, 4.47 and 2.92 kJ/mol were obtained for the reduction of GG, PB, BH, SJY, and YD, respectively. In all the cases, the reaction corresponded to the model function of $F_1(\alpha)$, and the integral form was $-\ln(1-\alpha)=kt$. Through this investigation, it could be concluded that the most appropriate ore category for sinter pot was YD.*

***Keywords:*** *Iron ore; Fluidity mechanism of ore; Reduction; Model function*

## 1. Introduction

The consumption amount of iron ore is increasing with the increase of iron and steel enterprise amount in China. The iron ore used is mainly divided into domestic and imported for iron and steel enterprise, and the price of the imported ore remains high. The sintering meets the great challenge: first, the sources and varieties of imported ores are diverse, and the results to the not ensure the metallurgical property of sinter; then, the used proportion of domestic iron ore, whose metallurgical performance is not stable, is increasing. The properties of iron ore mainly include ambient temperatures and high temperatures properties, and the high temperatures properties of iron ore are also called sintering basic characteristics. The sintering basic characteristics of iron ore mainly include fluidity, assimilation, bonding phase strength, etc., and they can influence the metallurgical properties of sinter. Thus, a lot of scholars study the relationship between the basic sintering characteristics of iron ore and the metallurgical performance of sinter.

Dong et al [1] investigated the effect of higher alumina iron ore of the gibbite type on the performance of sintering. They indicated that the ability of fluidity and melt formation were poor with the increase of the $Al_2O_3$ content of iron ore, and caused the poor metallurgical properties of sinter. The melt fluidity of iron ore depends on the liquid phase amount and viscosity, and can influence the sintering process [2]. Viscosity is also one of the important physiochemical properties of slag, and low viscosity could promote the efficiency of the desulfurization

**Corresponding author: jiangx@smm.neu.edu.cn*

***https://doi.org/10.2298/JMMB190221024G***

reaction of slag [3]. Additionally, the fluidity of iron ore increased with the increase of $SiO_2$ and the decrease of $Al_2O_3$. It had been demonstrated that Australian iron ore could influence the basic sintering characteristics [4]. With the increase of added amount of Australian iron ore, the main components of bonding phase changed: first, the silico-ferrite of calcium and aluminium (SFCA) phase transformed into kirschsteinite, silicate, and SFCA; then they changed into $2CaO{\cdot}SiO_2$ and SFCA. The Australian iron ore displayed better liquid fluidity ability, higher bonding phase strength and crystal strength, but poor assimilability. Some researchers indicated that fluidity index increased with the increase of low melting point liquid phase and $SiO_2$ content of iron ore [5]. The assimilation characteristics of iron ore could affect the fluidity and the bonding strength of sinter [6]. Many studies started to examine the effect of dolomite on the metallurgical properties of chromium-bearing vanadium-titanium magnetite sinter [7]. The flame front speed, sintering utilization factor, and the value of reduction degree decreased with the increase of MgO in sinter; however, the reduction disintegration index (RDI) and softening-melting properties enhanced. Magnetite, magnesium ferrite, and silicate increased with the increase of MgO content. Yang et al. studied the effect of typical specular hematite ores with distinct size distributions on the sintering performance, and found that the size distribution of iron ore could influence the performance of sintering: the ore of intermediate size displayed an inferior sintering performance; However, the metallurgical performance of sinter could be improved by mixing with other size distribution ores [8]. Zhang et al. evaluated the effect of $SiO_2$ in the ore on the metallurgical performance of sinter. They found that the reduction disintegration behavior of sinter was inhibited with the increase $SiO_2$ in the iron ore, and the main reason was that the amount of liquid phase increased with the increase of $SiO_2$ content [9]. In order to examine the influence of additives on the metallurgical properties of sinter, Raygan et al. studied the cold strength and the reduction behavior of sinters by adding talc and bentonite. They found that the sinter with talc could attain better cold strength, whereas the addition of bentonite could achieve better reduction [10]. Researchers attempted to evaluate the impact of particle size of limestone on metallurgical properties of sinter. In the case of the added limestone which was 1.25-1.52 mm in size, the sinter had higher strength and lower RDI, and the main reason was that the iron ore could attain better permeability in sintering process and more calcium ferrite phases appeared [11].

Earlier studies reported on the properties of iron ore and the quality of sinter. However, there is no unified understanding of the effect of $SiO_2$ on the fluidity of iron ore, and the main primary mechanism is not clear. The effect of fluidity of iron ore on the reduction of sinter still lacks deep theoretical insights. Therefore, this study mainly focused on the influencing mechanism of fluidity, and the reduction behavior of sinter by single iron ore sintering. In this study, the sinter pot index was analyzed, including particle size distribution, vertical sintering speed, and tumbler index. The reduction mechanism of sinter was tested by using SEM, XRD, and chemical composition analysis. The kinetic model had been used to describe the reduction mechanism of sinter. Finally, an appropriate category of iron ore was considered with an analysis of its principal component.

## 2. Materials and Methods

### *2.1 Characterization*

Sinters of different chemical compositions ($MgO/Al_2O_3$=0.71-2.32, $SiO_2$=4.12-8.48) were yielded by using sinter pot whose diameter was 300mm and 800mm in bed height. The chemical compositions of the iron ore and the fluxes are shown in Table 1. GG was hematite and it contained more $SiO_2$. BH was a mixture ore which came from Australian south mineral resources. PB was limonite and came from Australia; it had better sintering properties. YD was Australian limonite , and it had more crystal water which caused bad sintering properties. SJY was domestic hematite.

***Table 1.*** *Chemical composition of raw materials used in sinter pot %*

| Brand | | Chemical compositions | | | | | |
|---|---|---|---|---|---|---|---|
| | TFe | FeO | $SiO_2$ | CaO | MgO | $Al_2O_3$ | LOI |
| GG | 58.58 | 0.84 | 12.42 | 0.14 | 0.24 | 1.27 | 2.32 |
| BH | 62.06 | 0.15 | 6.35 | 0.005 | 0.17 | 1.27 | 2.36 |
| PB | 61.29 | 0.08 | 5.65 | 0.008 | 0.088 | 2.06 | 5.73 |
| YD | 57.15 | 0.08 | 7.00 | 0.02 | 0.13 | 1.43 | 10.32 |
| SJY(domestic) | 65.03 | 20.00 | 3.00 | 0.23 | 0.50 | 0.48 | 1.54 |
| Light burned dolomite | — | — | 3.60 | 42.12 | 24.38 | 1.35 | 27.24 |
| quicklime | — | — | 3.90 | 73.75 | 2.69 | 1.82 | 16.65 |

The size distribution of different raw materials is shown in Table 2. SJY was a fine ore with 96.31% passing 0.2 mm, 100% passing 1 mm; however, YD was a coarse ore with only 8.37% passing 0.2 mm, and 29.91% passing 1 mm. The experimental method of sintering basic characteristics was introduced in relevant literature; the paper will not repeat the description [12-14].

***Table 2.*** *Size distribution of raw materials %*

| | <0.2mm | 0.2-1mm | >1mm |
|---|---|---|---|
| GG | 49.84 | 15.83 | 34.33 |
| BH | 36.64 | 35.89 | 27.48 |
| PB | 23.06 | 29.33 | 47.61 |
| YD | 8.37 | 21.54 | 70.09 |
| SJY | 96.31 | 3.69 | 0.00 |
| Light burned dolomite | 45.52 | 32.65 | 21.83 |
| quicklime | 41.66 | 33.64 | 24.71 |

### *2.2 Thermodynamic consideration*

During the raw materials sintering for the sinter pot experiment, the following reaction may occur:

$$2C + O_2 = 2CO \quad (1)$$

$$2CO + O_2 = 2CO_2 \quad (2)$$

$$CaCO_3 = CaO + CO_2 \quad (3)$$

$$CaMg(CO_3)_2 = CaO + MgO + 2CO_2 \quad (4)$$

$$4Fe_3O_4 + O_2 = 6Fe_2O_3 \quad (5)$$

The reaction (1) was the coke gasification reaction, (2) was the CO oxidation, (3) was the limestone decomposition, (4) was the light burned dolomite decomposition, and (5) was the magnetite oxidation. The relationship between Gibbs free energy change and the temperature of reaction (1)-(5) is shown in Fig 1. As can be seen from Fig 1, the (2) and (5) were the exothermic reactions, the Gibbs free energy was increased with the reaction temperature increase. In the case of the reaction temperature above 1200K, the reactions (2) and (5) cannot occur. The reactions (1), (3), and (4) were endothermic reactions, the Gibbs free energy was decreased with the decomposition temperature increase. In the case of the reaction temperature below 811K, the reaction (1), (3), and (4) cannot occur.

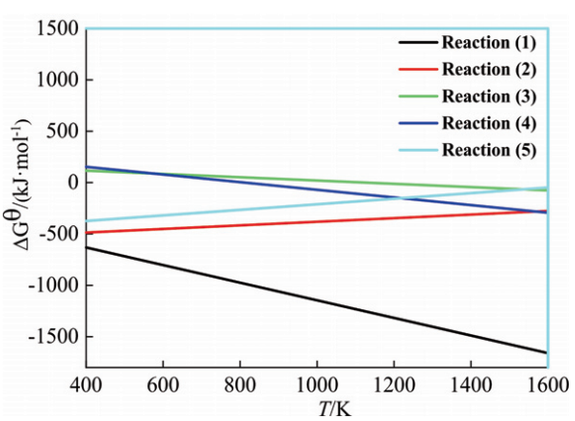


***Figure 1.*** *Relationship between Gibbs free energy change and temperature of reaction (1)-(5)*

The main chemical reaction of the sintering process was endothermic, as reaction (1), (3) and (4) show, and the exothermic reaction was only a small part in the sintering process, as shown in reaction (2) and (5). The higher reaction temperature was beneficial to the sintering process, so the higher ignition temperature (1073K) was advantageous for the reaction in the sintering process.

### *2.3 Sintering*

The raw materials used in the single iron ore sintering experiment included ore, return fines, coke, and sintered coal, and they were 52.64 kg, 22.14 kg, 1.79 kg and 1.79 kg, respectively; the basicity was fixed at 1.9 (binary basicity). The experiment of sinter pot mainly included six parts: mixture, granulation, charging, ignition, sintering, and cooling. The detailed operating parameters of sinter pot test are shown in Table 3. The mixture was loaded into the sinter pot after mixing, the mixing times was twice: once was mixing materials and twice was granulating. The ignition time and temperature were 2 min and 1073 K, respectively. In the case of the coal gas temperature reached its peak value and appeared downtrend, the experiment reached the end point. After the experiment finished, the cold air was pumped into the sinter pot and then immediately discharged, the main purpose simulated the actual situation of sintering production field. The crushed sinter was dropped from 2 m, 3 times, and sieved into six different particle size: <6.3, 6.3-10, 10-16, 16-25, 25-40, >40.

***Table 3.*** *Experiment condition of sinter pot*

| Item | Parameter | Item | Parameter |
|---|---|---|---|
| Ignition suction | 7.5kPa | Sintering suction | 13kPa |
| Ignition time | 2min | Bed height | 700mm |
| Ignition temperature | 1073K | Mass of Hearth Layer | 3kg |
| Moisture | 6.0±0.5% | | |

The main sintering parameters were calculated as:

$$V = H / t \quad (6)$$

$$n_a = \frac{M_3 - 4}{(M_1 - M_2)(1 - H_2O\%)} \times 100\% \quad (7)$$

$$n_{np} = \frac{M_4 - 4}{M_3 - 4} \times 100\% \quad (8)$$

$$DI = \frac{M_5}{7.5} \times 100\% \quad (9)$$

Where, $V$ is the vertical sintering speed, mm/min;

$H$ is the layer height, mm; $t$ is the sintering time, min; $n_a$ is yield, %; $M_1$ is the weight of raw materials after mixing and added water, kg; $M_2$ is the weight of residual raw material after pouring into sinter pot, kg; $M_3$ is the weight of sinter after the end of the experiment, kg; $n_{np}$ is the productivity, %; $M_4$ is the weight of sinter with the particle size greater than 5 mm after fall and screening, kg; $DI$ is the tumbler index, %; $M_5$ is the weight of sinter with particle size greater than 6.3 mm after the tumbler experiment.

### *2.4 Reduction*

Reduction test was carried out in a dilatometer as shown in Fig 2. The experiment set-up mainly comprises six facilities: a gas system, a desiccant, a computer system, a thermocouple, an electric furnace, and a flowmeter. The inert atmosphere was maintained by blowing nitrogen gas, the reduction furnace was 800mm in height and 75mm in diameter. The size of the sinter was 10~12.5mm, the experiment temperature was 1073K, 1173K, and 1273K, which was controlled at ±10K. In order to illustrate the properties of sinter under industrial conditions, all tests were operated in a constant reduction

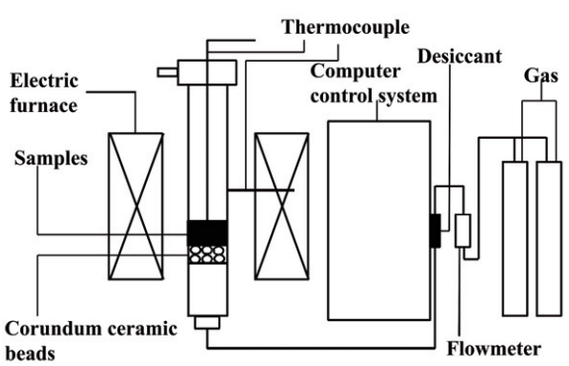


***Figure 2.*** *Schematic diagram of the reduction test device*

atmosphere. The reduction gas was a mixture of CO and $N_2$, and gas composition was set at CO=30% (0.27m$^3$/h) and $N_2$=70% (0.63m$^3$/h). The flowing of shielding gas was 0.3m$^3$/h, with the purpose to prevent oxidation.

The reduction degree is calculated as the fraction of oxygen removed from the sinter. However, the oxides containing Mg, Si, and Ca can hardly be reduced under the experimental temperature and atmosphere conditions in the study. Therefore, the reduction degree (α) is generally treated as the mass percentage of oxygen removed from the iron oxides and was evaluated as:

$$\alpha = \frac{m_1 - m_t}{m_0} \tag{10}$$

Where, $m_1$ is the initial mass of sinters, g, $m_t$ is the mass of sinters after reduction time t, g, $m_0$ is the total mass of oxygen theoretically capable to be removed, g.

In the Eq. (10), the total mass of removable oxygen in the sinters is evaluated assuming that all the oxygen of the combining iron exists in the form of $Fe_2O_3$; however, some $Fe_3O_4$ and FeO also occurred in the sinters. The reduction degree should be calculated according to the mass loss in the experiment and the difference between the theoretical mass of oxygen and the actual weigh of oxygen. In the paper, the actual weight of oxygen is calculated according to $Fe_2O_3$, $Fe_3O_4$ and FeO existing in the sinters, and the reduction degree can be evaluated according to the Eq (11)

$$\alpha = \frac{m_0 W_1 \times \frac{8}{71.85}}{m_0 W_2 \times \frac{48}{111.7}} \times 100 + \frac{m_1 - m_t}{m_0 \times \frac{W_2}{100} \times \frac{48}{111.7}} \times 100 \tag{11}$$

Eq (11) is simplified into the form of Eq. (12)

$$\alpha = \left( \frac{0.111 W_1}{0.430 W_2} + \frac{m_1 - m_t}{m_0 \times 0.430 W_2} \times 100 \right) \times 100 \tag{12}$$

Where $W_1$ is the wustite (FeO) content before reduction, %; $W_2$ is the total iron (TFe) content before reduction, %; 0.111 and 0.430 is necessary conversion.

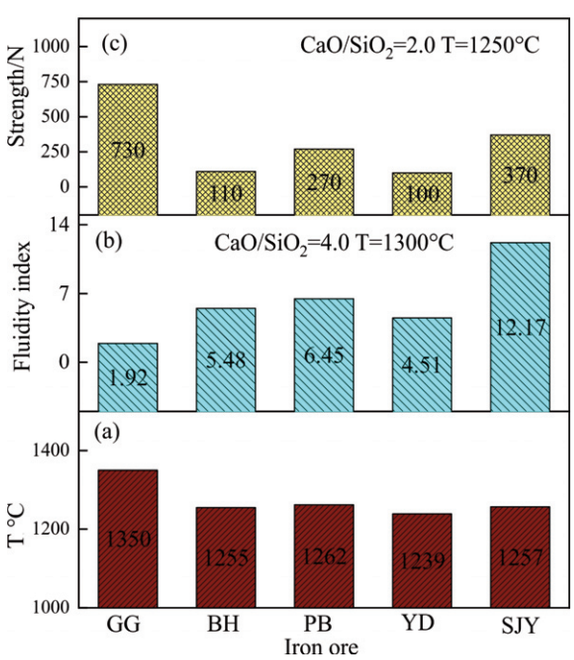


***Figure 3.*** *The sinter basic characteristic of different ore (a: assimilation temperature; b: liquidity index; c: bonding phase strength)*

## 3. Results

### *3.1 Sintering basic characteristics*

The sintering basic characteristics for different iron ore were carried out as shown in Fig 3. The assimilability refers to the ability that iron ore reacts with the calcium (CaO) during the process of sintering. It reflects the difficulty degree generating a melt, and the evaluation index of the assimilation characteristic of iron ore is the assimilation temperature. The assimilation temperature of SJY was lower (1259°C), and could generate more bonding phases. However, the GG had higher assimilation temperature (1350°C).

The effect of $SiO_2$ content on the assimilation temperature is shown in Fig 4. The $SiO_2$ content had a quadratic relationship with the assimilation temperature as shown in Eq. (13).

$$A = 2.15M^2 - 23.90M + 1315.29 \quad (13)$$

Where, $A$ is the assimilation temperature (°C), and $M$ is the $SiO_2$ content (%).

The assimilation temperature decreased with the increase of $SiO_2$ content. When the $SiO_2$ reached the lowest point of the quadratic function, i.e., YD, the assimilation temperature was the lowest, then the temperature increased with the increase of $SiO_2$ content. The eutectic mixture, $CaO{\cdot}SiO_2$-$CaO{\cdot}Fe_2O_3$-$CaO{\cdot}2Fe_2O_3$, with a melting point of 1192 °C is formed, and a small part of the eutectic mixture ($2FeO{\cdot}SiO_2$-$2CaO{\cdot}SiO_2$) with a melting point of 1150 °C is formed with the increase of $SiO_2$ content of iron ore [14]. With the further increase of $SiO_2$ content, the formation of the iron silicate occurs, which cannot react with calcium oxide. Based on the above analysis, a small amount of $SiO_2$ contributes to the decrease of assimilation temperature, but an excessive $SiO_2$ increases the assimilation temperature.

The bonding phase strength refers to the ability of the liquid phase to combine ore nuclei in the sintering process, and the properties determine the strength of sinter under certain conditions of sintering. The bonding phase strength of GG, BH, and YD were 730 N, 110 N, and 100 N, respectively, and the trend was gradually decreased with the change of iron ore from GG to SJY. There are two main reasons for the highest bonding phase strength of GG: (1) In the case when the basicity is 4.0 ($CaO/SiO_2$=4.0), the higher $SiO_2$ in the ores means the increase of the ratio of CaO, and the contact area of CaO and iron oxide increases. This condition is useful to the formation of low melting point liquid phase; (2) The basic oxide can separate the network structure of silicon-oxygen anion to simpler silicon-oxygen complex anion. The content of crystal water in YD is the highest, so the decomposition of crystal water can lead to the formation of cracks and pores in the bonding phase, and results in the lowest bonding phase strength for YD.

The fluidity index is an important parameter; it demonstrates the flowing capacity of ore melts in the sintering process and expresses the effective bonding range of the melt. The fluidity index of SJY (12.17) and PB (6.45) were higher than GG, BH, and YD; the main reason was the appropriate $SiO_2$ content. The BH and YD had a relatively higher fluidity index (5.48, 4.51), and the fluidity index of GG was lowest (1.92). The main reason for different fluidity of ores will be explained in the Section 4.1.

### *3.2 Results of sinter pot*

Fig 5 shows the changes that occur during the operating parameters of the sintering process with single iron ore. The vertical sintering speed of SJY was the lowest in all the cases, which had sufficient reaction time to bond with other raw materials of sintering. GG had a relatively fast vertical sintering speed and resulted in poor metallurgical properties of sinter. The vertical sintering speeds of GG and SJY were 33.13 and 11.23 $mm{\cdot}min^{-1}$, respectively. The tumbler index of GG was the lowest (55.82%) and that of SJY was the highest (61.41%). In the case of

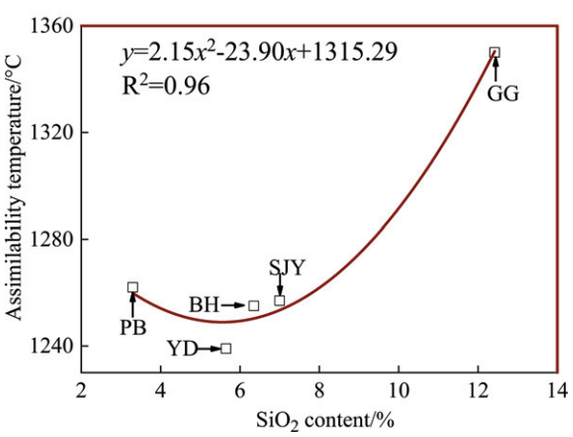


***Figure 4.*** *The effect of $SiO_2$ on the assimilation temperature*

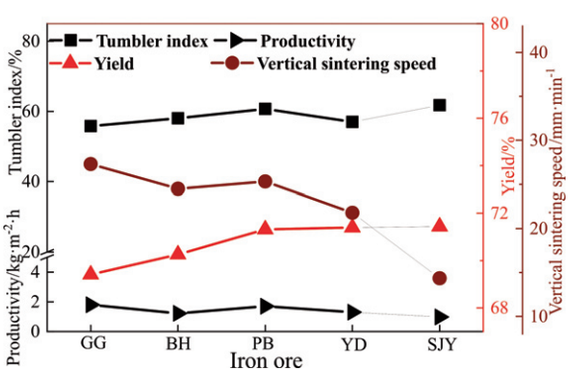


***Figure 5.*** *Effect of single iron ore on results of sintering process*

the iron ore changed from GG to SJY, the productivity decreased from 1.8 to 0.98 kg·m$^{-2}$·h, and the yield increased from 69.41 to 71.44%. The GG contained more $SiO_2$ and caused the increase of the liquid phase in the sintering process, which led to lower tumbler strength for GG. The particle size of SJY was fine, and caused bad permeability of material layer in the sintering process. In the case of the SJY used, the tumbler index was higher and the vertical sintering speed was lower. The YD belonged to limonite, and the ore contained more crystal water. The decomposition of crystal water might deplete the heat for sinter process. These circumstances could make the raw material of sintering attain less heat and lower strength for YD.

The size distribution of sinter for different single iron ore is shown in Fig 6. GG contained more larger size particles (>40 mm, 18.37%) and smaller size particles (<6.3 mm, 27.74%). However, the larger and smaller particles were less for YD i.e. particles of >40 mm and <6.3 mm were 7.67% and 30.59%, respectively. The poor fluidity and higher assimilative temperature could cause poor size distribution for GG, and the better sintering basic characteristics (fluidity, assimilative temperature) led to the better size distribution for YD.

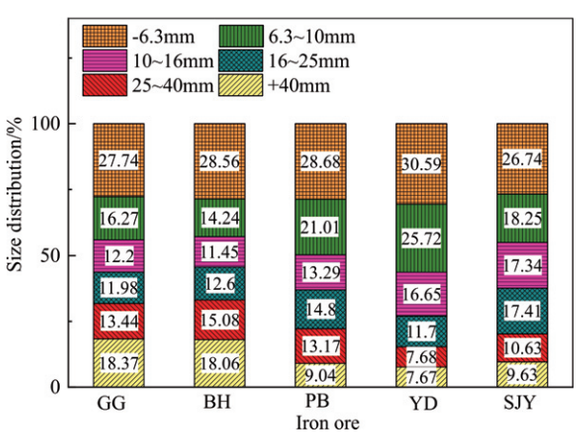


***Figure 6.*** *The size distribution of sinter for single iron ore*

XRD analysis was conducted to confirm the phase composition of sinter for the different blending of ores. Scanning was carried out from 10° to 80° at a scan rate of 6°/min. X-ray analysis of the applied sinters exhibits the principal mineral phase which contained hematite, magnetite, calcium ferrite, and iron silicon oxide as shown in Fig 7. The formation of magnetite and calcium ferrite was suppressed, and other mineral chemicals had insignificant variations from GG to SJY. The sintering temperature and the MgO content caused the differences mineral composition of sinter.

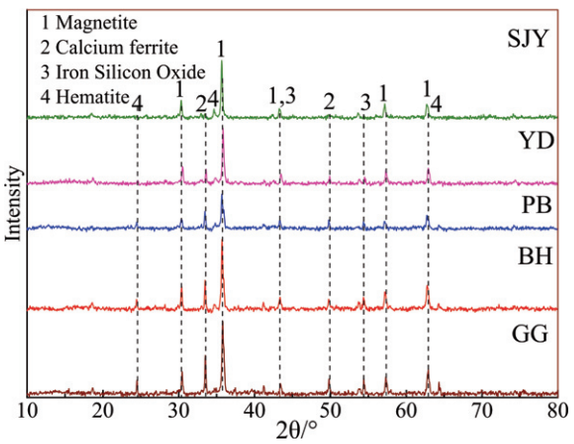


***Figure 7.*** *XRD profile of the sinter sample for different ore*

### *3.3 Results of reduction degree*

A comparison of the reduction curves at the same temperature is given in Fig 8. It can be seen that the reduction degree increased with the increase of the

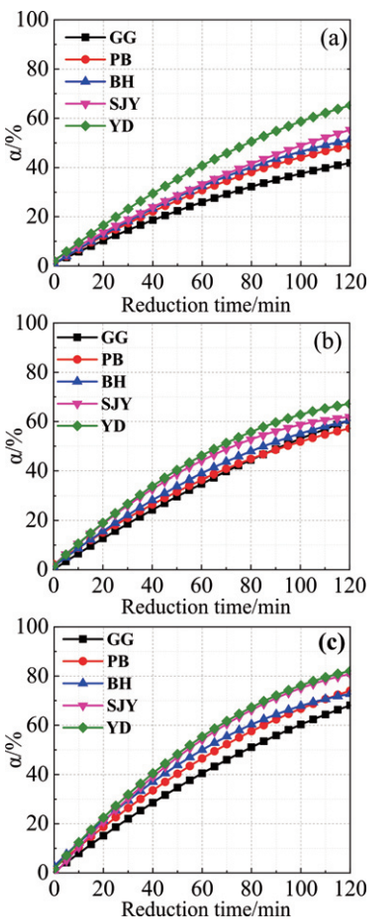


***Figure 8.*** *Relationship between reduction degree and reduction time with different raw materials (a) 1073K (b) 1173K (c) 1273K*

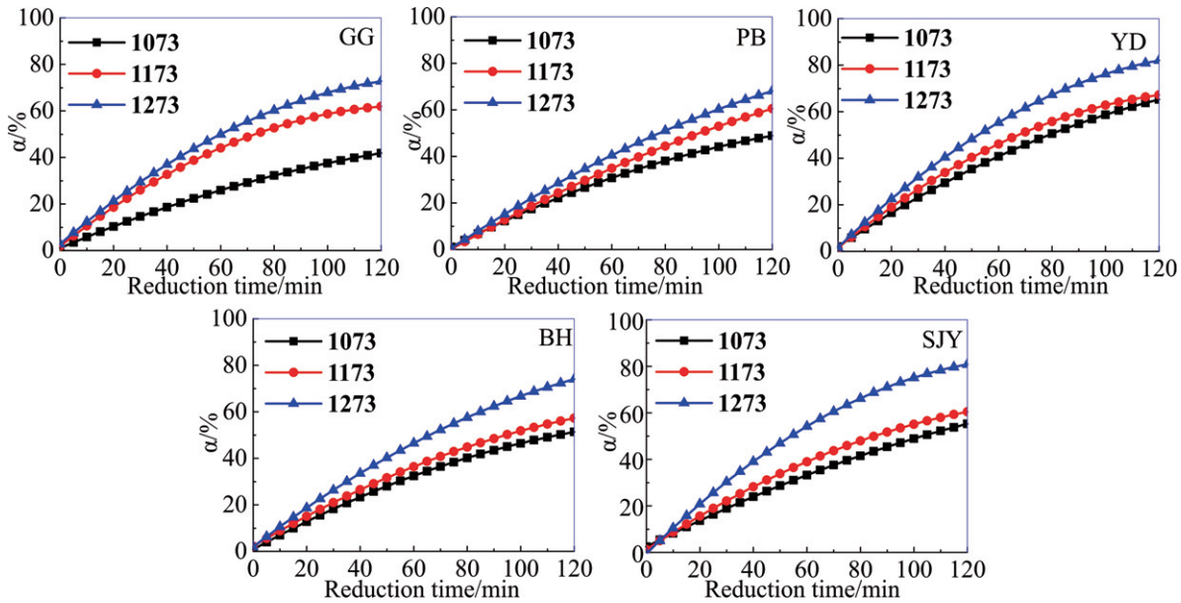


***Figure 9.*** *Relationship between reduction degree and reduction time at different temperature*

reduction time in all the cases. When the reduction temperature was 1073 K, 1173 K, and 1273 K, the reduction degree of YD showed the highest value and that of GG showed the lowest value. The reduction degree of YD was obviously higher than other sinters at 1073 K, but slightly larger than other samples at 1173 K and 1273 K. When the temperature was 1073 K and the time was 120 min, the reduction degree of YD was about 20% higher than that of GG; However, the reduction degree of YD was only 10% higher than that of GG at 1173 K and 1273 K.

Typical reduction curves of sinters isothermally reduced with GG, PB, BH, SJY, and YD at different temperatures (1073-1273K) are given in Fig 9. In all the cases, the reduction degree curves of sinter increased with the increase of the applied temperature. The maximum reduction degree of GG was 41% at 1073 K and 73% at 1273 K. The maximum reduction degree of YD was 65% at 1073 K and 82% at 1273 K. The performance of different reduction might have been caused by chemical composition, microstructure, mineral composition, etc.

To clarify the mechanism of isothermal reduction of sinter for different raw materials, and comparison between the results of experiments at different temperatures and raw materials, the XRD patterns of GG and YD at 1073 K and 1173K were obtained, as shown in Fig 10. When GG was reduced at 1073 K for 60 min, the main mineral components were wustite (FeO), magnetite ($Fe_3O_4$), calcium ferrite ($CaO{\cdot}Fe_2O_3$), metallic iron (Fe), and a small amount of hematite ($Fe_2O_3$); the hematite ($Fe_2O_3$) gradually disappeared after 120 min. The main components of YD were wustite (FeO) and metallic iron (Fe) at 60 min and 120 min. The metallic iron (Fe) increased with the increase of the reduction temperature for GG. The obtained results of XRD correlate well with the results of the reduction degree.

## 4. Discussion

### *4.1 Effect of $SiO_2$ on the mechanism of fluidity of ore*

The samples of $CaO\text{-}SiO_2\text{-}Fe_2O_3$ system were

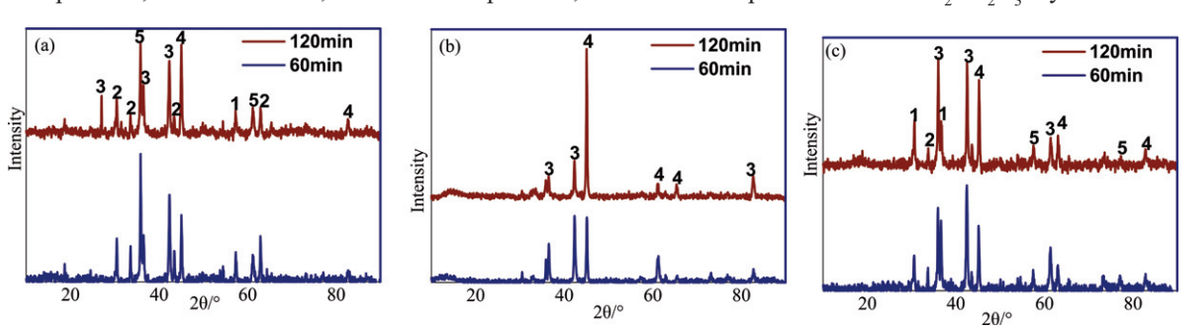


***Figure 10.*** *XRD pattern of sinter at different stages (a: GG in 1073K b:YD in 1073K c: GG in 1173K):1- $Fe_2O_3$;2-$Fe_3O_4$; 3-FeO; 4-Fe; 5-$CaO{\cdot}Fe_2O_3$*

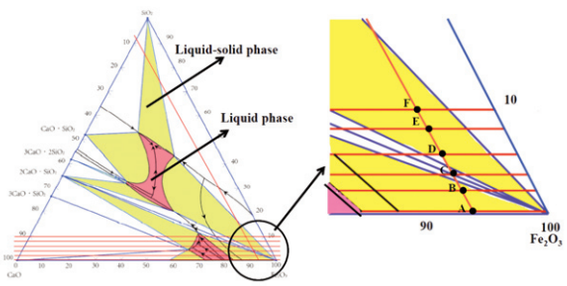


***Figure 11.*** *The isothermal section of phase diagram for CaO-$SiO_2$-$Fe_2O_3$ at 1300°C (A: $SiO_2$=0%; B: $SiO_2$=2%; C: $SiO_2$=4%; D: $SiO_2$=6%; E: $SiO_2$=8%; F: $SiO_2$=10%)*

roasted by using chemical reagents: CaO content was 8%, $SiO_2$ content was 0, 2, 4, 6, 8, and 10%, respectively and the rest was $Fe_2O_3$. The isothermal section of the phase diagram for CaO-$SiO_2$-$Fe_2O_3$ at 1300 °C is shown in Fig 11. The A-F point in this figure corresponded to 0-10% of $SiO_2$ content. When the sintering process reached the equilibrium reaction, the liquid phase decreased with the increase of $SiO_2$ content, i.e., the liquid phase amount was 48% and 28% for 0% and 10% $SiO_2$ content, respectively. However, the sintering time was short and the reaction did not reach the equilibrium; thus, the amount of liquid phase could not attain the theoretical value. In the non-equilibrium state, the effect of $SiO_2$ on the liquid phase amount is shown in Fig 12 (roasting time: 4 min; roasting temperature: 1300 °C).

The main phase of minerals was hematite and liquid phase, the gray part was hematite and the black part was a liquid phase as shown in Fig 12. The amount of liquid phase gradually increased. The liquid phase was connected, then changed into a large scale. The liquid phase separated the hematite, and the shape was irregular for lower $SiO_2$ content. The hematite gradually integrated into a whole, and the shape was more regular with the increase of $SiO_2$ content.

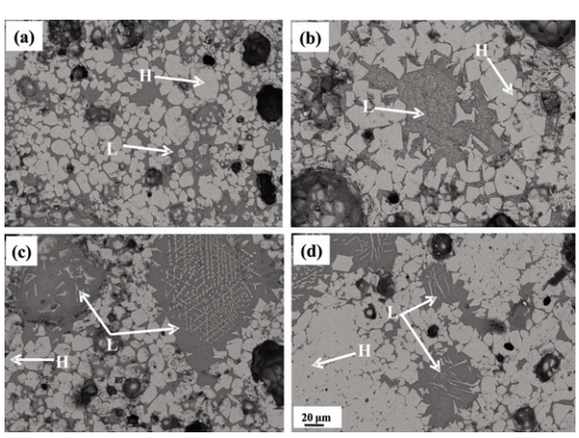


***Figure 12.*** *The effect of $SiO_2$ on liquid phase: (a) $SiO_2$=4% (b) $SiO_2$=6% (c) $SiO_2$=8% (d) $SiO_2$=10% L: Liquid phase; H: Hematite*

The minerals compositions of samples for different $SiO_2$ contents are shown in Fig 13. The hematite was 65.09% for 4% $SiO_2$. However, the hematite content steeply decreased with the increase of $SiO_2$ content, i.e. 61.59%, 49.68%, and 41.56%, for the $SiO_2$ contents of 6%, 8%, and 10% , respectively. The liquid phase was 34.9%, 38.41%, 50.32%, and 58.44% for the $SiO_2$ contents of 4%, 6%, 8%, and 10%, respectively. The liquid phase sharply increased with the increase of $SiO_2$ content. In the non-equilibrium state, the liquid phase increased with the increase of $SiO_2$ content, and led to a better fluidity of iron ore.

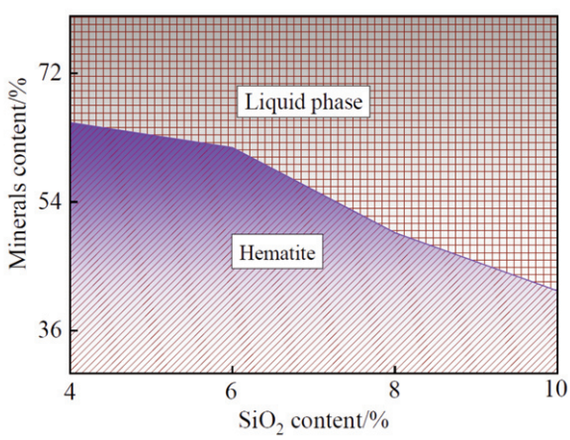


***Figure 13.*** *The effect of $SiO_2$ on liquid phase: (a) $SiO_2$=4% (b) $SiO_2$=6% (c) $SiO_2$=8% (d) $SiO_2$=10% L: Liquid phase; H: Hematite*

The effect of $SiO_2$ on the melting point of CaO-$SiO_2$-$Fe_2O_3$ system is shown in Fig. 14. It can be seen that the melting point of CaO-$SiO_2$-$Fe_2O_3$ system decreased with the increase of SiO2. The melting point was 1511 °C, 1487 °C for the $SiO_2$ contents of 0% and 10%, respectively, and the melting point decreased by 24 °C with the $SiO_2$ content increased from 0 to 10%. The $SiO_2$ could lead to the decrease of

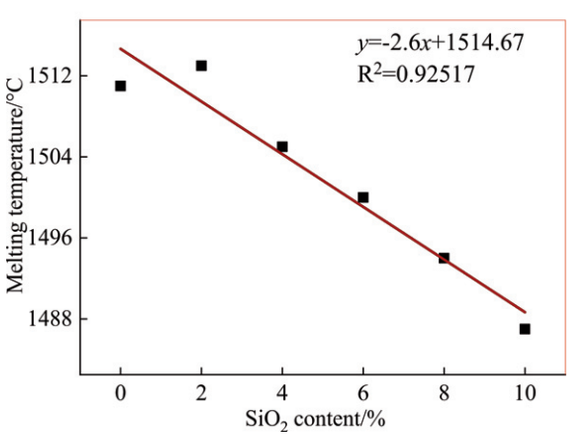


***Figure 14.*** *The effect of $SiO_2$ on the melting temperature*

melting point, which was also a significant reason for the excellent fluidity of iron ore containing more amount of $SiO_2$.

The $SiO_2$ content of GG was the highest, but its fluidity index was the lowest, and fluidity was the poorest. To understand the above phenomena, the sample was analyzed by SEM, and the microstructure is shown in Fig 15. GG mainly contained two phases ($Fe_2O_3$ and liquid phase) after roasting. The liquid phase was the primary phase, and $Fe_2O_3$ was relatively less. The $Fe_2O_3$ showed the dendrite shape uniformly distributed between the liquid phases, and then the liquid phase connected into a whole. It can be seen from the energy spectrum analysis that $SiO_2$ mainly existed in the liquid phases, and did not enter into $Fe_2O_3$. With the increase of $SiO_2$ in the ore, the higher amount liquid phase could lead to incomplete crystallization in the cooling process and then the secondary hematite appeared in the iron ore. Based on the above reasons, the fluidity of GG was poor.

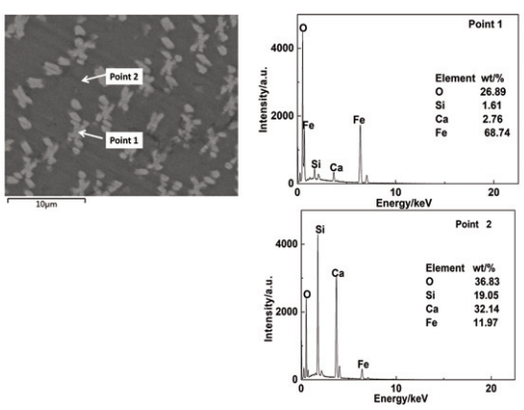


***Figure 15.*** *Energy spectrum analysis of GG*

The fluidity of the liquid phase was also inferior with the increase $SiO_2$ content, and the ion theory of slag could analyze its main influencing mechanism. The silicon dioxide could form a silicate ion or ion cluster, which were strong acid and complex structure in slag. Their chemical structure is shown in Fig 16.

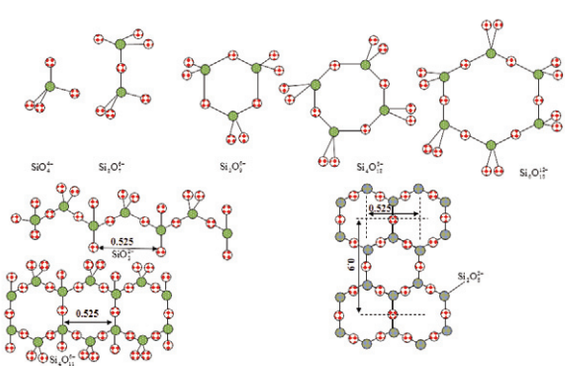


***Figure 16.*** *Diagram of the structure of $SiO_2$ complex anion*

The silica-oxygen compound anion was the most critical complex anion in the silicate. The $SiO_4^{4-}$, which was the basic unit of tetrahedral structure, located in the void of the tetrahedral structure formed by $O^{2-}$. For the slag of low $SiO_2$ content, the $SiO_4^{4-}$ was separated by cationic and there was an ionic bond between $SiO_4^{4-}$ with cation. It was necessary to consume $O^{2-}$ to change into complex ion. With the increase of $SiO_2$ content, the intense polymerization of $SiO_4^{4-}$ and $O^{2-}$ could lead to a complicated complex ion. The reactions are shown in Eq. (14), (15) and (16).

$$SiO_2 + O^{2-} = SiO_4^{4-} \quad (14)$$

$$SiO_4^{4-} + SiO_4^{4-} = Si_2O_7^{6-} + O^{2-} \quad (15)$$

$$3SiO_4^{4-} = Si_3O_{10}^{8-} + 2O^{2-} \quad (16)$$

With the increase of polymerization of $SiO_4^{4-}$, the shared $O^{2-}$ increased and the structure of silicon-oxygen ion was more complicated. The structure of point, line, and surface gradually developed to body. In other words, the radius of the structure and the volume of ion cluster increased with the increase in the tetrahedral structure. Finally, a skeleton-like anion group was formed, and they formed by the connection of infinite tetrahedrons composed of pure $SiO_2$. This was another reason why the higher $SiO_2$ in the iron ore caused poor fluidity.

Therefore, the fluidity index first increased and then decreased with the increase of $SiO_2$ content of iron ore. There were two significant reasons for the increase of fluidity index: first, $SiO_2$ could cause the increase liquid phase amount in the sample, and second, it decreased the melting point of the sample. As the $SiO_2$ content increased further, the fluidity index of iron ore decreased. A higher $SiO_2$ led to an incomplete crystallization of hematite, and appeared secondary hematite, thus its fluidity index decreased. On the other hand, an excessive $SiO_2$ decreased the fluidity of the liquid phase itself, which could be explained by the ion theory of slag.

### *4.2 Changes in the morphology*

It is well-known that the microstructure of sinter is an essential factor of affecting its reduction. Fig 17 shows the SEM image of a polished cross-section of the sinter by adding different categories of ores. All the microstructures were taken at similar magnification to ensure that the distribution of grains and sizes were captured. It could be seen that the sinter mainly contained two phases: hematite and liquid phase, and the liquid phase compositions of different sinter were different.

When the category of single iron ore was GG, the hematite was distributed in point, the liquid phase was

surrounded by the hematite. The hematite was divided by the liquid phase, and the distributed state caused poor crystallization ability of hematite. Based on the above reason, the hematite cannot connect to form a flake area. The main composition of liquid phase was calcium silicate ($CaO \cdot SiO_2$), but calcium ferrite ($CaO \cdot Fe_2O_3$) did not appear. The main reactions for the liquid phase are shown in Eq. 17-19 in the sintering process. Also, the relationship between Gibbs free energy change and the temperatures of reactions for Eq. (17)-(19) are shown in Fig 18.

$$CaO+Fe_2O_3=CaO \cdot Fe_2O_3 \quad (17)$$

$$2CaO+Fe_2O_3=2CaO \cdot Fe_2O_3 \quad (18)$$

$$CaO+SiO_2=CaO \cdot SiO_2 \quad (19)$$

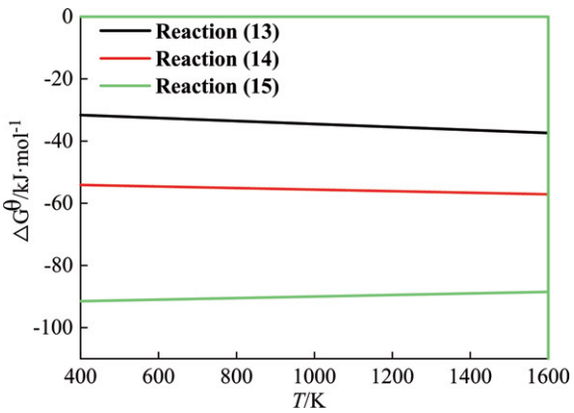


***Figure 18.*** *The relationship between Gibbs free energy change and temperature*

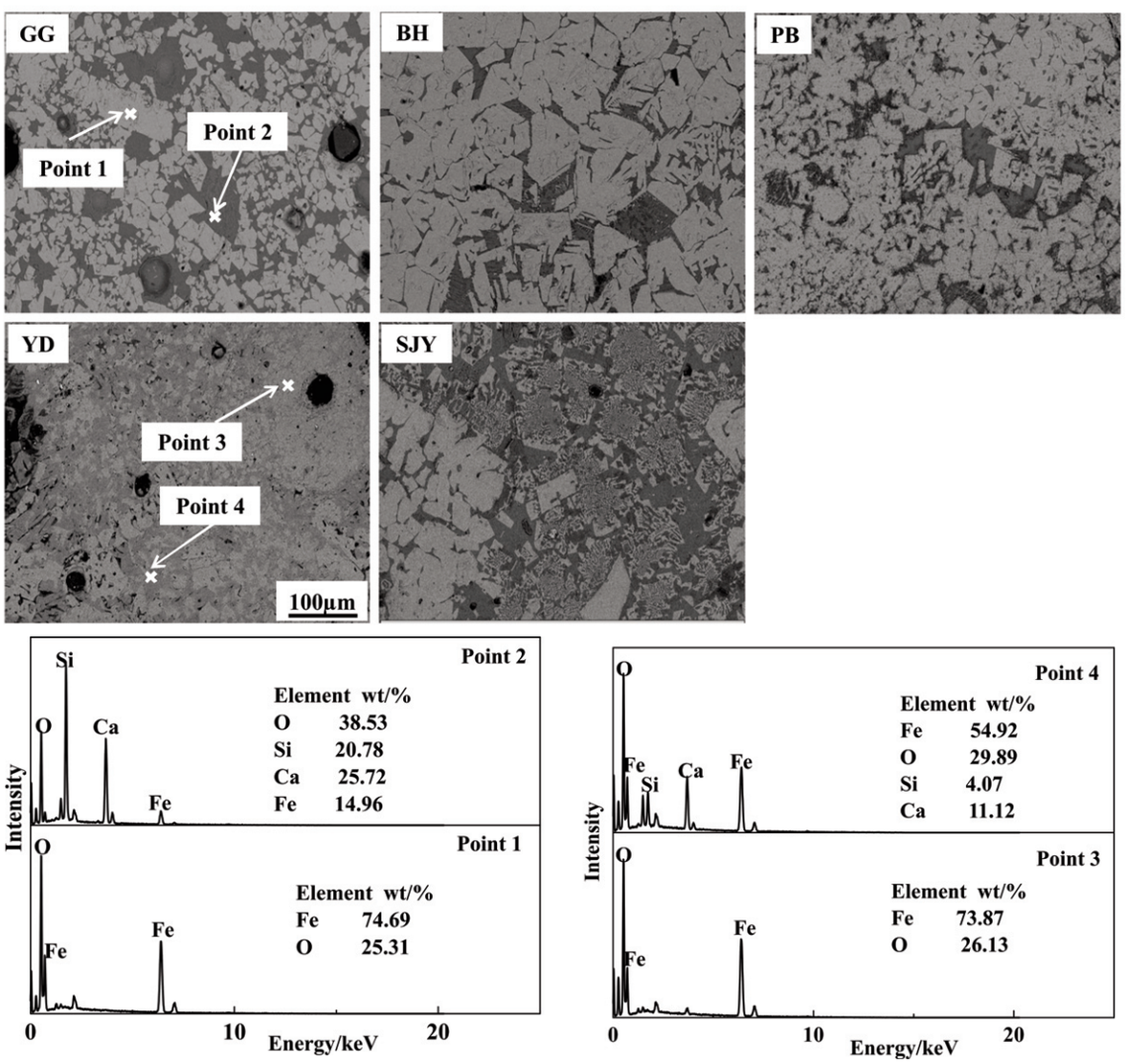


***Figure 17.*** *SEM image and EDS analysis of sinter with single iron ore*

The Gibbs free energy of calcium ferrite ($CaO·Fe_2O_3$) and dicalcium ferrite ($2CaO·Fe_2O_3$) was higher than that of calcium silicate ($CaO·SiO_2$) in the temperature ranges of 400-1600 K. When the $SiO_2$ content in iron ore was enough, the CaO first reacted with $SiO_2$ and formed $CaO·SiO_2$; with the decrease of $SiO_2$ content of iron ore, the CaO reacted with $Fe_2O_3$ and formed $CaO·Fe_2O_3$ and $2CaO·Fe_2O_3$.

For BH and PB, the amount of liquid phase decreased with the decrease of $SiO_2$ content of iron ore. The hematite was connected and formed a flat structure, and the type of crystal transformed from the initial euhedral crystal to interconnected crystal.

When the category of single iron ore was YD, there was no calcium silicate; however, a lot of calcium ferrite (light gray part) appeared. The liquid phase played a proper bonding role so that the hematite was fully bonded and the crystal was sufficiently grown.

When the category of single iron ore was SJY, the degree of crystallization of hematite was relatively high. They existed in the form of interconnected crystal, but the compositions of liquid phase were more complex. The main liquid phase region was examined for its elemental distribution, as shown in Fig 19. It could be noted that the calcium silicate shown skeletal distribution and a small amount of magnesium oxide existed in the calcium silicate, and the hematite located in between the liquid phase. The composition and structure of the sinter contributed to the increase reduction, and its mechanism requires further analysis and discussion.

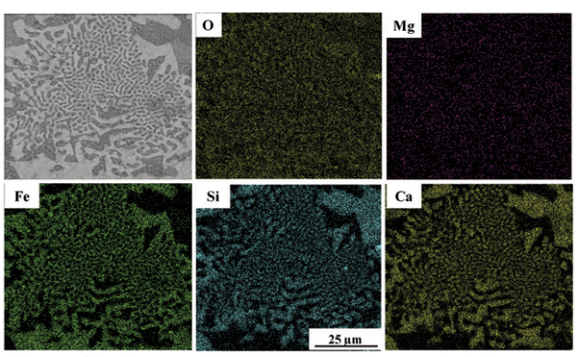


***Figure 19.*** *Element distributions of sinter with SJY*

### *4.3 Kinetic analysis of reduction*

The kinetic results obtained were useful to establish the reduction mechanism as follows. The relationship between reduction rate and time could be expressed by the dynamic differential equation of heterogeneous phase systems, as shown in Eq. (20)

$$\frac{d\alpha}{dt} = k(T)f(\alpha) \tag{20}$$

Where, dα/dt is the reduction rate and *k(T)* is the reaction rate constant, f(α) is the mode function describing the reaction mechanism. *k(T)* conforms to the Arrhenius, as shown in Eq. (21)

$$k(T) = A\exp(\frac{-E}{RT}) \tag{21}$$

Where, *A* is pre-exponential factor, *E* is the apparent activation energy, and *R* is the gas constant [8.314J/(mol·K)]. Eq. (22) is further expressed as

$$\frac{d\alpha}{dt} = A\exp(\frac{-E}{RT})f(\alpha) \tag{22}$$

The mode function integral form is Eq. (23)

$$G(\alpha) = \int_0^\alpha \frac{d\alpha}{f(\alpha)} = \int_0^t A\exp(\frac{-E}{RT})dt = k(T)t \tag{23}$$

Model functions were determined according to lnln analysis method [15]. On the basis of the Avami-Erofeev, the kinetics of reduction degree was carried out the method [16]. The equation of Avami-Erofeev is shown in Eq. (24) and (25)

$$1-\alpha = \exp^{-kt^n} \tag{24}$$

$$\ln\left[-\ln(1-\alpha)\right] = n\ln t + \ln k \tag{25}$$

Where *α* is the reduction degree of samples (%) and *n* is judgment index of model function. Obtaining the double natural logarithm on either side of the equal sign of Eq. (24), we could formulate the following equation (25). The *n* could interpreter the model function of different reactions. The main model functions are shown in Table 4 [15].

Fig 20 shows the linear fitting results of the ln(-ln(1-α)) to lnt for different sinters at different

***Table 4.*** *The relationship of model function and judgment index*

| Function | Kinetic model | equation | *n* |
|---|---|---|---|
| $D_1(\alpha)$ | One-dimensional diffusion | $\alpha^2=kt$ | 0.62 |
| $D_2(\alpha)$ | Two-dimensional diffusion | $(1-\alpha)\ln(1-\alpha)+\alpha=kt$ | 0.57 |
| $D_3(\alpha)$ | Three-dimensional diffusion | $[1-(1-\alpha)1/3]^2=kt$ | 0.54 |
| $A_1(\alpha)$ | Avarmi-Erofeev, n=1 | $[-\ln(1-\alpha)]^{1/2}=kt$ | 2 |
| $A_2(\alpha)$ | Avarmi-Erofeev, n=2 | $[-\ln(1-\alpha)]^{1/3}=kt$ | 3 |
| $F_1(\alpha)$ | First-order reaction | $-\ln(1-\alpha)=kt$ | 1 |

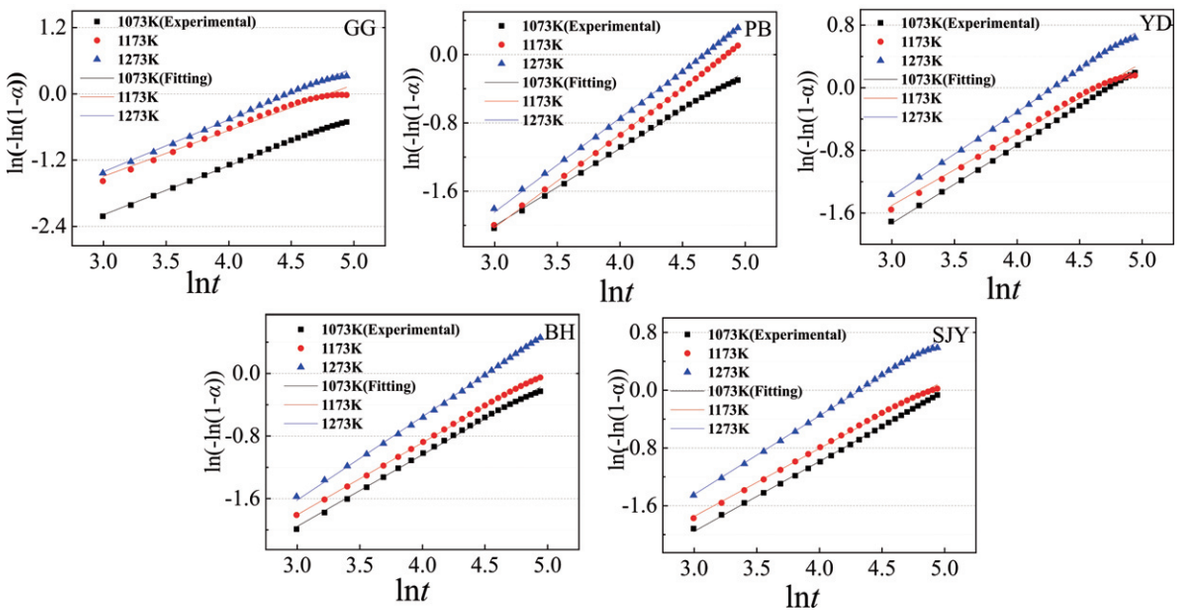


***Figure 20.*** *Plot of ln(-ln(1-α)) vs lnt for different raw materials*

temperatures and the Table 5 shows the slope (*n*) of the linear fitting and the degree of fitting ($R^2$). The degree of fitting about was 0.99 and the results are reasonable. The average value of slope (*n*) was 0.93926, 1.02698, 0.97913, 1.01508, and 1.01847, respectively, for GG, PB, BH, SJY, and YD. The results indicated that the experimental data for GG, PB, BH, SJY, and YD mostly lie on the standard curve corresponding to the function $F_1(\alpha)$ and the integral form was $-\ln(1-\alpha)=kt$. Therefore, the reaction of different raw materials could be described by mode function $F_1(\alpha)$.

***Table 5.*** *The slope of linear fitting and $R^2$*

| Item | *T*/K | Slope, *n* | $R^2$ |
|---|---|---|---|
| GG | 1073 | 0.91508 | 0.99988 |
| | 1173 | 0.91755 | 0.99902 |
| | 1273 | 0.98516 | 0.99988 |
| PB | 1073 | 0.93476 | 0.99988 |
| | 1173 | 106.891 | 0.99978 |
| | 1273 | 107.728 | 0.99962 |
| BH | 1073 | 0.94986 | 0.99986 |
| | 1173 | 0.93944 | 0.99992 |
| | 1273 | 104.809 | 0.99934 |
| SJY | 1073 | 0.95547 | 0.9995 |
| | 1173 | 0.97211 | 0.99994 |
| | 1273 | 111.765 | 0.99989 |
| YD | 1073 | 0.99628 | 0.99971 |
| | 1173 | 0.97316 | 0.99975 |
| | 1273 | 108.597 | 0.99951 |

The Arrhenius equation method was used to calculate the activation energy for obtained the activation energy under different reactions. The rate constant *k*(T) was obtained by finding the plots of G(a) against time *t*, and the fitting result are shown in Fig 21. Table 6 shows the *k*(T) of the linear fitting and the degree of fitting ($R^2$). It was indicated that the fitting degree of the different reaction was higher than 0.99, the accuracy of the fitting result was high. The reaction rate constant was increased with the increased temperature.

***Table 6.*** *Rate constant and the degree of fitting*

| Item | T/K | *k*/T | $R^2$ |
|---|---|---|---|
| GG | 1073 | 0.00449 | 0.99785 |
| | 1173 | 0.0083 | 0.99042 |
| | 1273 | 0.01103 | 0.99888 |
| PB | 1073 | 0.0056 | 0.99815 |
| | 1173 | 0.00773 | 0.99827 |
| | 1273 | 0.00949 | 0.99747 |
| BH | 1073 | 0.00605 | 0.9983 |
| | 1173 | 0.00702 | 0.99947 |
| | 1273 | 0.01113 | 0.99785 |
| SJY | 1073 | 0.00654 | 0.99976 |
| | 1173 | 0.00781 | 0.99909 |
| | 1273 | 0.01426 | 0.99866 |
| YD | 1073 | 0.00874 | 0.99968 |
| | 1173 | 0.00955 | 0.99702 |
| | 1273 | 0.01457 | 0.99809 |

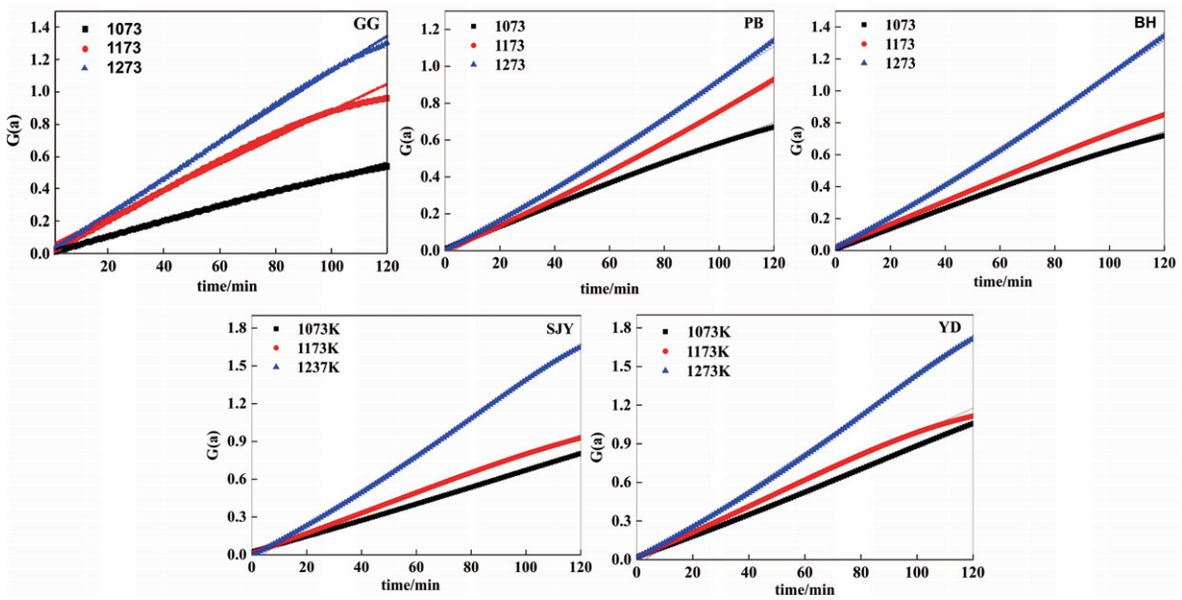


***Figure 21.*** *Plot of G(a) vs time for sinter with single iron ore*

The reaction rate constant to the temperature was obtained by the Arrhenius equation, which can calculate the activity energy of the chemical reaction, the equal is shown in (26) and (27).

$$k = Ae^{\frac{-Ea}{RT}} \tag{26}$$

$$\ln k = \ln A - \frac{Ea}{RT} \tag{27}$$

Where $k$ is the constant of the reaction rate, $A$ is the pre-exponential factor, $Ea$ is the activation energy, $T$ is the temperature. The activation energy can be obtained by the slope of fitting of ln$k$ (T) against 1/$T$ in the Fig 22, the activation energy $Ea$ and the pre-exponential factor are shown in Table 7. The average activation energy was 5.39, 3.14, 3.51, 4.47, and 2.92kJ/mol$^{-1}$, and the pre-exponential was 1.92, 0.19, 0.29, 0.91, and 0.22min$^{-1}$, respectively, for GG, PB, BH, SJY, and YD. The activation energy of YD was the lowest, which indicated that the substance needed the lowest energy to change from a normal to active state which was prone to chemical reactions, and that of GG was the highest. Therefore, YD had the best reduction and that of GG was the worst.

***Table 7.*** *Activation energy and pre-exponential factor of different sinter*

| | GG | PB | BH | SJY | YD |
|---|---|---|---|---|---|
| E/(kJ·mol$^{-1}$) | 5.39 | 3.14 | 3.51 | 4.47 | 2.92 |
| A/min$^{-1}$ | 1.92 | 0.19 | 0.29 | 0.91 | 0.22 |

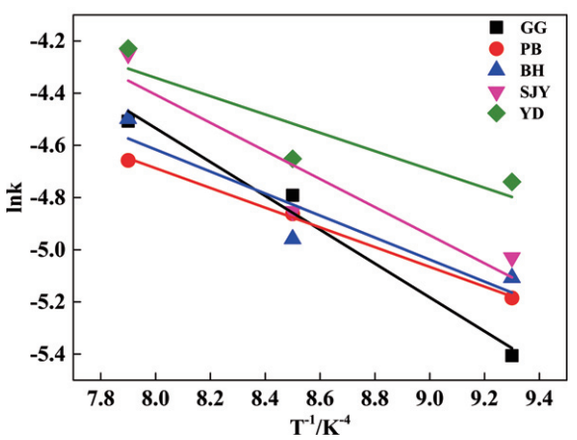


***Figure 22.*** *The effect of reduction degree on activation energy*

### *4.4 Comprehensive assessment index of the metallurgical properties*

The properties of sinter could be improved by an appropriate ore category. The principal component analysis (PCA) was used to analyze the ore. The method was used to corroborate the composite indicator of sinter. The appropriate ore category was calculated by the PCA. The calculation process by the PCA was detailed below.

The parameters of the sinters as follows: primitive matrix=X; canonical matrix=X'; covariance matrix=C; eigenvector of canonical matrix=λ

The original data could constitute the primitive matrix, that the date was assimilative temperature, bonding phase strength, fluidity index, vertical sintering speed, tumbler index and reduction degree

of different temperature at 120 min. The primitive matrix is shown in (28).

$$X=\begin{bmatrix} x_{11} & x_{12} & \cdots & x_{1p} \\ x_{21} & x_{22} & \cdots & x_{2p} \\ x_{31} & \ddots & \vdots & x_{3p} \\ x_{n1} & x_{n2} & \cdots & x_{np} \end{bmatrix} \tag{28}$$

The primitive matrix was calculated by normalized, where the average value of the disposing matrix maintained constant. The canonical matrix is shown in Eq. (29), (30)

$$X^{\square}=\begin{bmatrix} a_{11} & a_{12} & \cdots & a_{1p} \\ a_{21} & a_{22} & \cdots & a_{2p} \\ a_{n1} & a_{n2} & \vdots & a_{np} \end{bmatrix} \tag{29}$$

$$a_{ij}=\left(x_{ij}-\bar{x}_j\right)/\sqrt{\frac{1}{n}\left(x_{ij}-\bar{x}_j\right)^2}, i=1,2,\cdots n; \bar{x}_j = \frac{1}{n}\sum_{i=1}^{n}x_{ij}, j=1,2,\cdots,p \tag{30}$$

The covariance matrix was defined as generalized from random variables of scalar to high dimensional. The calculation results of the covariance matrix are shown in (31) and (32)

$$C=\begin{bmatrix} \mathrm{r}_{11} & r_{12} & \cdots & r_{1p} \\ r_{21} & r_{22} & \cdots & r_{2p} \\ r_{p1} & r_{p2} & \vdots & r_{pp} \end{bmatrix} \tag{31}$$

$$r_{jk}=\sum_{i=1}^{n}\left(a_{ij}-\overline{a_j}\right)\left(a_{ik}-\overline{a_k}\right)/\sqrt{\sum_{i=1}^{n}\left(a_{ij}-\overline{a_j}\right)^2\sum_{i=1}^{n}\left(a_{ik}-\overline{a_k}\right)^2}, \quad i=1,2,...n, j,k=1,2,...p, \overline{a_j}=1/n\sum_{i=1}^{n}a_{ij} \tag{32}$$

The corresponding eigenvector of the maximum eigenvalue is selected as the matrix of dimensionality reduction as shown in (33).

$$P=\begin{bmatrix}69.45 & 22.02 & 6.28 & 2.25\end{bmatrix}' \tag{33}$$

The comprehensive assessment of the metallurgical properties for different MgO content pellets is shown in equation (34).

$$Y=PX'=\begin{bmatrix}4.34 & 26.59 & 143.25 & 270.34 & 68.8\end{bmatrix} \tag{34}$$

Fig 23 shows the comprehensive assessment index of different ores. The best evaluation results of the ores were YD.

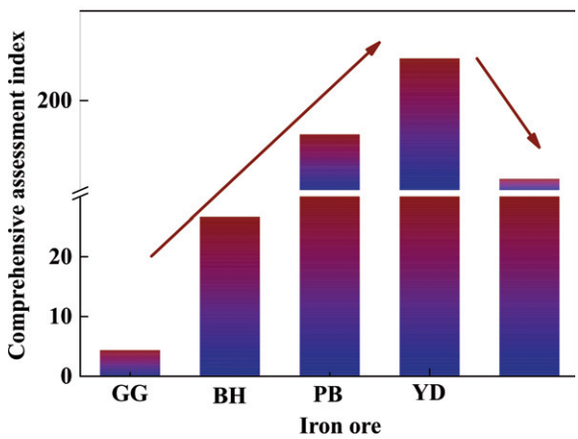


***Figure 23.*** *The effect of ore category on comprehensive assessment index*

## 5. Conclusions

In this fundamental study, the sintering basic characteristics of different categories of iron ore were examined, and the sinter pot was conducted for five types single iron ore sintering. Finally, the reduction of five types sinter was measured by the loss mass. The obtained results from this investigation are summarized as follows:

1. The fluidity index first increased and then decreased with the increase of $SiO_2$ content in the iron ore. The main reason for the increase fluidity index of iron ore was that the amount of liquid phase increased and the melting point decreased. However, the poor fluidity for liquid phase and the appearance of secondary hematite caused the decrease of fluidity index of iron ore.

2. The main bonding phase of sinter was calcium silicate and hematite for the higher $SiO_2$ content and calcium ferrite and hematite for the lower $SiO_2$. The main reason was that the Gibbs free energy of calcium ferrite and dicalcium ferrite ($2CaO{\cdot}SiO_2$) was greater than that of calcium silicate in the temperature ranges of 400-1600 K.

3. During the reduction time of 120min, the reduction degree of YD was the highest in all the cases, they reached 64.23%, 66.37%, and 81.12%, at 1073 K, 1173 K and 1273 K, respectively, and GG was the lowest, which reached 42.74%, 62.49%, and 72.64%, respectively.

4. The kinetic analysis indicated that the reaction corresponded to the model function of $F_1(\alpha)$ and the integral form was $-\ln(1-\alpha)=kt$. The average activation energies were 5.39, 3.14, 3.51, 4.47, and 2.92 kJ/mol, and their pre-exponential factors were 1.92, 0.19, 0.29, 0.91, and 0.22 $min^{-1}$, for GG, PB, BH, SJY, and YD, respectively.

5. The comprehensive assessment index was increased and then decreased with the change from

GG to SJY, and the appropriate category of iron ore was YD.

**Acknowledgments**

*The authors wish to acknowledge the contributions of associates and colleagues at the Northeastern University of China. Also, the financial support of National Science Foundation of China (NSFC 51774071) is very much appreciated.*

**Reference**

[1] J. J. Dong, G. Wang, Y. G. Gong, Q. G. Xue, J. S. Wang, Ironmak. Steelmak., 42 (1) (2015) 34-40.

[2] S. L. Wu, X. B. Zhai, Metall. Res. Technol., 115 (2018) 1-16.

[3] K. Ouyang, Z. H. Dou, T. A. Zhang, Y. Liu, J. Min. Metall. Sect. B-Metall., 56 (1) (2020) 27-33.

[4] D. H. Liu, H. Liu, J. L. Zhang, Z. J. Liu, X. Xue, G. W. Wang, Q. F. Kang, Int. J. Miner. Metall. Mater., 24 (9) (2017) 991-998.

[5] P. Jun, Z. Lei, X. L. Li, L. A. Sheng, Metall. Mater. Trans. B., 48 (1) (2017) 538-544.

[6] S. L. Wu, G. L. Zhang, S. G. Chen, B. Su, ISIJ Int., 54 (3) (2014) 582-588.

[7] S. T. Yang, W. D. Tang, M. Zhou, T. Jiang, X. X. Xue, W. J. Zhang, Minerals, 7 (12) (2017) 210-225.

[8] C. C. Yang, D. Q. Zhu, B. J. Shi, P. Jian, L. M. Lu, X. B. Li, Y. P. Mo, J. Iron Steel Res. Int., 24 (10) (2017) 1007-1015.

[9] Q. J. Zhang, Y. L. Li, X. G. Ma, Z. M. Cui, Y. Z. Zhang, Applied Mechanics and Materials, 275-277(2013) 1874-1877.

[10] S. Raygan, H. Abdizadeh, A. Dabbagh, M. Pourabdoli, Ironmak. Steelmak., 36 (4) (2009) 273-278.

[11] T. Umadevi, U. K. Bandopadhyay, P. C. Mahapatra, M. Prabhu, M. Ranjan, Steel Res. Int., 81 (6) (2010) 419-425.

[12] M. Zhou, T. Jiang, S. T. Yang, X. X. Xue, Int. J. Miner. Process., 142 (2015) 125-133.

[13] S. L. Wu, H. L. Han, H. X. Li, J. Xu, S. D. Yang, X. Q. Liu, Int. J. Miner. Metall. Mater., 17 (1) (2010)11-16.

[14] D. H. Liu, J. L. Zhang, Z. J. Liu, Y. Z. Wang, X. Xue, J. Yan, JOM, 68 (9) (2016) 2418-2424.

[15] J. D. Hancock, J. H. Sharp, J. Am. Ceram. Soc., 55 (2010) 74-77.

[16] M. Avrami, J. Chem. Phys., 7 (1939) 1103-1112.

# UTICAJ KONCENTRATA RUDE ŽELEZA NA KARAKTERISTIKE SINTEROVANJA I REDUKCIJU SINTERA

**H. Guo [a], F.-M. Shen [b], X. Jiang [b,*], D.-W. Xiang [b], H.-Y. Zheng [b]**

[a] Hebei severni univerzitet, Džangđiakou, Hebei, Kina
[b] Metalurški fakultet, Severnoistočni univerzitet, Šenjang, Liaoning, Kina

***Apstrakt***

*Kako je Australija glavna zemlja iz koje Kina uvozi rudu železa, bogata mineralna nalazišta u Australiji su za Kinu primarni izvor sirovih materijala za sinterovanje. Kako bi se bolje razumele osobine različitih ruda železa iz Australije kao i proces sinterovanja, u ovoj studiji izabrano je četiri tipa rude iz Australije i jedna iz Kine, i njihove osobine su ispitivane pod različitim uslovima. Da bi se ispitao uticaj različitih ruda železa na metalurške osobine sintera, proučavan je eksperiment u kome je sinterovana pojedinačno svaka ruda železa. Iz ovog eksperimenta dobijeni su sledeći rezultati: GG ruda je pokazala slabu fluidnost i višu temperaturu asimibilnosti, ali je vezna čvrstoća bila najveća; YD ruda je pokazala bolju fluidnost i nižu temperaturu asimibilnosti, dok je SJY (ruda iz Kine) pokazala bolju fluidnost i veću snagu vezne čvrstoće kao i nižu temperaturu asimibilnosti. Mehanizam uticaja rude železa na fluidnost dalje je analiziran uz pomoć SEM kao i jonske teorije obrazovanja šljake. Sa povećanjem $SiO_2$ sadržaja u rudi, indeks fluidnosti je rastao, a glavni razlog je to što je tokom sinterovanja količina tečne faze rasla a tačka topljenja je opadala. Ipak, prevelika količina $SiO_2$ bila je uzrok pada indeksa fluidnosti rude železa, a glavni razlog je taj što je fluidnost same tečne faze opadala i pojavio se sekundarni hematit. U slučaju kada je $SiO_2$ sadržaj rude bio veći, glavna faza očvršćavanja je bio kalcijum silikat. Sa smanjenjem $SiO_2$ sadržaja, kalcijum silikat se transformisao u kalcijum ferit. Glavni razlog je to što je Gibsova slobodna energija kalcijum ferita i dikalcijum ferita ($2CaO•SiO_2$) bila veća od one kalcijum silikata u temperaturnom rasponu od 400-1600 K. Stepen redukcije YD je u svim slučajevima bio najveći, a stepen redukcije GG najmanji. Aktivacione energije od 5.39, 3.14, 3.51, 4.47 i 2.92 kJ/mol dobijene su za GG, PB, BH, SJY i YD, pojedinačno. U svim slučajevima, reakcija je korespondirala sa modelom funkcije $F_1(\alpha)$, a integralni oblik je bio $-\ln(1-\alpha)=kt$. Putem ovog istraživanja moglo se zaključiti da je YD najpogodnija kategorija rude za lonce za sinterovanje.*

***Ključne reči:*** *Ruda železa; Mehanizam fluidnosti rude; Redukcija; Model funkcije*